Resolution-enhanced three-dimensional image reconstruction by use of smart pixel mapping in computational integral imaging

Dong-Hak Shin,[1] Chun-Wei Tan,[1] Byung-Gook Lee,[1]
Joon-Jae Lee,[2,*] and Eun-Soo Kim[3]

[1]Department of Visual Contents, Dongseo University, San69-1, Jurye2-Dong, Sasang-Gu, Busan 617-716, Korea

[2]Department of Game Mobile Contents, Keimyung University, Daemyung3-Dong Nam-Gu, Daegu 705-701, Korea

[3]Department of Electronics, Kwangwoon University, 447-1, Wolge-Dong, Nowon-Gu, Seoul 139-701, Korea

*Corresponding author: joonlee@kmu.ac.kr

Received 13 June 2008; revised 17 September 2008; accepted 30 October 2008;
posted 10 November 2008 (Doc. ID 97274); published 8 December 2008

Computational integral imaging method can digitally provide a series of plane images of three-dimensional (3D) objects. However, the resolution of 3D reconstructed images is dramatically degraded as the distance from the lenslet array increases. In this paper, to overcome this problem, we propose a novel computational integral imaging reconstruction (CIIR) method based on smart pixel mapping (SPM). Since SPM is a computational process in which elemental images recorded at long distances are convertible to ones recorded near lenslet array, this can give us the improved resolution of plane images for 3D objects located at a long distance range from a lenslet array. For the effective use of the SPM-based CIIR method, we design a novel two-stage CIIR method by the combined use of the conventional CIIR and the SPM-based one. The conventional CIIR method is applied over a short distance range, while the SPM-based CIIR is used over a long distance range. We carry out some experiments to verify the performance of the two-stage CIIR system. From the experimental results, the proposed system can provide a substantial gain over a long distance range in terms of the resolution of reconstructed plane images.

OCIS codes: 100.6890, 110.2990, 110.4190.

1. Introduction

Recently, integral imaging has been studied for three-dimensional (3D) imaging, television, and visualization [1–8]. It can produce the autostereoscopic images with full parallax and continuous viewing points. An integral imaging system is composed of two processes: pickup process and reconstruction process as shown in Figs. 1(a) and 1(b). In integral imaging, the lenslet array is used in both processes to capture 3D objects and reconstruct 3D images. In the pickup process, the light rays coming from 3D objects are passing through the lenslet array and recording a set of different perspective images by using an image sensor. These recorded images are referred to as elemental images (EIs). In the reconstruction process, a similar lenslet array as in the pickup process is used. By back-propagating light rays of the EIs through lenslet array, the 3D images are formed at the location where it was picked up.

In the case of using the optical reconstruction process, the image quality of reconstructed image is poor due to the diffraction and limitation of the physical devices [5–7]. For the better 3D visualization and recognition, several types of computational reconstruction methods have been reported [9–13]. One of these computational reconstructions is a computational integral imaging reconstruction (CIIR) technique, which can produce a series of plane images using

0003-6935/08/356656-10$15.00/0

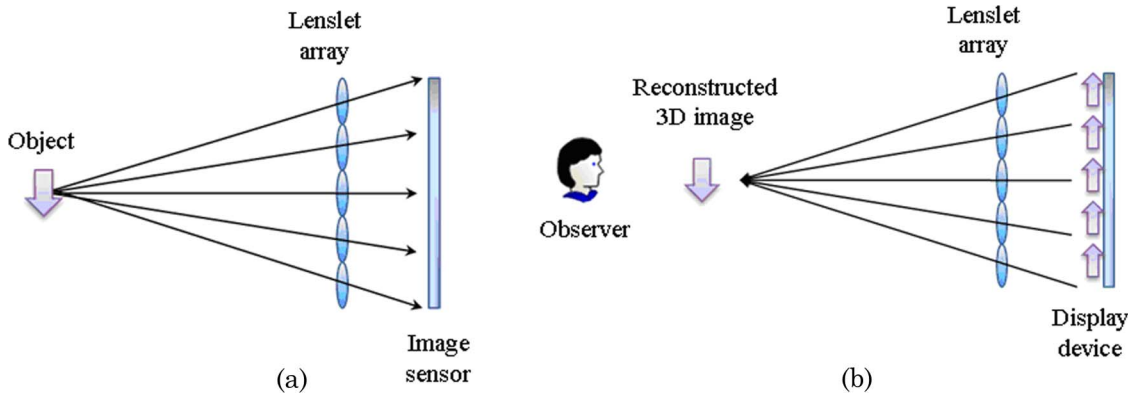

Fig. 1. (Color online) General integral imaging system: (a) pickup process and (b) reconstruction process.

the recorded EIs [13]. The recorded EIs are inversely mapped to an output plane and magnified according to a magnification factor. By summing all magnified EIs, plane images are finally reconstructed.

In the CIIR method, however, there are some serious problems such as artifacts of reconstructed plane images and the high computational load due to a large magnification factor at a far distance. There is quite a lot of research focusing on how to improve the resolution of plane images in CIIR [14–23]. Even though many approaches were applied to CIIR, the resolution degradation of plane images over the large depth range from the lenslet array was not dramatically improved. Basically, large depth requires large magnification factor, so a lot of overlapping process incurs interference among adjacent pixels when magnified EIs are superimposed on each other in CIIR [23].

In this paper, we propose a novel CIIR method based on smart pixel mapping (SPM) to improve the resolution of plane image over long distance. SPM is a computational depth-reverse process in which original EIs are convertible to ones recorded at the different pickup distance [24]. Based on this principle of SPM, the EIs recorded at the long distance can be converted to ones recorded near the lenslet array. This can give us the improved resolution of plane images and the reduction of computational time because of reducing the interference problem by short distance between lenslet array and target output plane. For the effective use of the SPM-based CIIR method, we designed a novel two-stage CIIR method by the combined use of the conventional CIIR and the SPM-based one. The conventional CIIR method is applied over a short distance range, while the SPM-based CIIR is used over a long distance range. We carry out some experiments to verify the performance of the two-stage CIIR system and present the results.

2. Review of Computational Integral Imaging

The computational integral imaging (CII) system shown in Fig. 2 is composed of two processes. The first process is the pickup process of 3D objects, and second one is the CIIR using EIs. In the pickup process of CII, EIs are recorded using a lenslet array and an image sensor. On the other hand, the CIIR process provides a series of plane images within a specific depth range by reconstructing plane images at any arbitrary distance from the lenslet array.

The concept of CIIR can be examined by using Fig. 2(b). Let the (p,q)th EI be E_{pq}. In order to reconstruct a plane image, EIs are inversely mapped to an output plane located in longitudinal distance z. The mapped EIs on the output plane are magnified with respect to a magnification factor, M, which is defined as the ratio of the distance between output plane and synthesized pinhole array, to the distance between EIs and synthesized pinhole array, g, that is, $M = z/g$. Then the inverse mapped image $R_{pq}{}^{z}$ of E_{pq} at the distance z is written as

$$R_{pq}^{z}(x,y) = \left(\frac{g}{z}\right)^{2} E\left(\frac{-gx}{z} + \left(1+\frac{g}{z}\right)s_x p, \frac{-gy}{z} + \left(1+\frac{g}{z}\right)s_x q\right) \times \text{for} \begin{cases} s_x(p - z/2g \le x \le s_x(p + z/2g) \\ s_y(q - z/2g \le y \le s_y(q + z/2g) \end{cases}, \quad (1)$$

where s_x and s_y are the size of an EI in the x and y directions, respectively. The reconstructed plane image $R^{z}(x,y)$ at the output plane z can be expressed as the summation of all the inversely mapped EIs and given by

$$R^{z}(x,y) = \sum_{p=0}^{m-1}\sum_{q=0}^{n-1} R_{pq}^{z}(x,y), \quad (2)$$

where m and n indicate the number of EIs in the x and y directions, respectively. Because of the magnification for each inversely mapped EI, superposition occurs for $M > 1$. And the overlapping numbers of inversely mapped EIs to reconstruct a certain pixel may be different from the corresponding numbers used to reconstruct the adjacent pixels. These variations in intensity generate the degradation of the quality of the reconstructed images. Therefore the

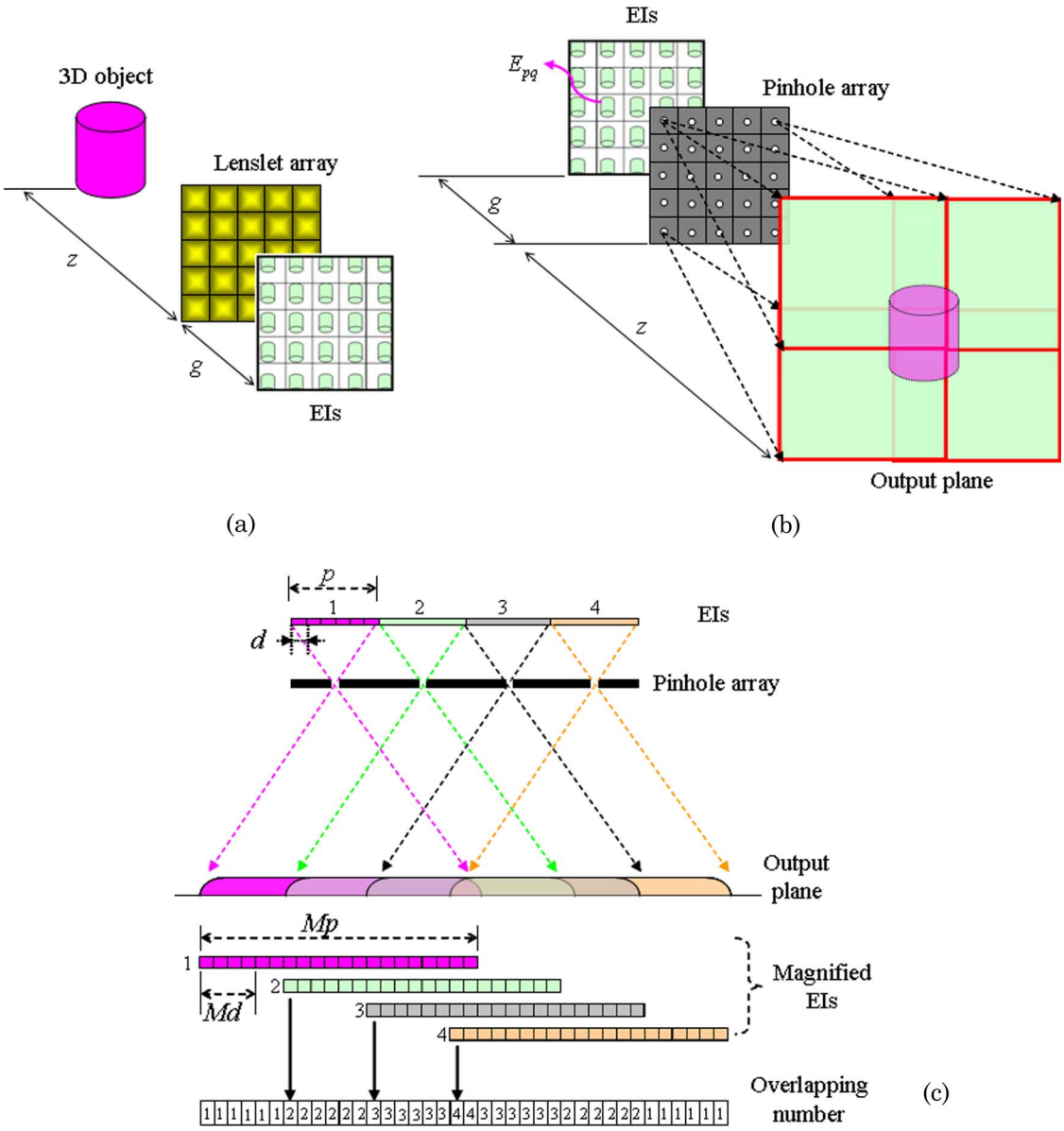

Fig. 2. (Color online) CII system: (a) pickup process, (b) CIIR process, and (c) superimposition example for four EIs.

compensation process is required. To do so, we count the overlapping number $N^z(x,y)$ for each pixel. The normalized plane image is given by

$$R^z_{\text{normal}}(x,y) = \frac{R^z(x,y)}{N^z(x,y)}. \tag{3}$$

To understand the superposition process of CIIR in detail, we assume four EIs as shown in Fig. 2(c). Then each EI is digitally magnified by a magnification factor $M = z/g$. Let us define the pixel size of EIs as d. Then the pixel size of the magnified EIs must increase to be Md. In the output plane, the distance between each magnified EIs is the pitch size p of the pinhole array. The magnified EIs are overlapped and summated with each other on the output plane as shown in Fig. 2(c). Here we can calculate the overlapping number by considering all positions of the EIs. In the center part of the output plane, the overlapping number is high. Otherwise, it becomes smaller. In addition we can see that CIIR requires high computational cost since the number of pixels to be calculated for magnification and superposition of EIs increases dramatically.

3. Proposed Two-Stage Computational Integral Imaging Reconstruction Method

A. Computational Integral Imaging Reconstruction Based on Smart Pixel Mapping

Even though the normalization of the reconstructed plane image is used in the previous CIIR method, it cannot avoid the resolution degradation of reconstructed images by interference due to a large magnification factor at a long distance. The interference

problem in the CIIR method is well explained in [23]. This causes the unwanted superposition of intensity information from adjacent pixels when the magnified EIs are summated in the output plane. Thus the interference amount largely increases as the magnification factor depending on distance z increases. To reduce the interference in CIIR, reducing distance z would be a good solution. In this paper, we propose a novel CIIR method based on SPM to improve the resolution of plane image over a long distance range.

The principle of SPM-based CIIR method is illustrated in Fig. 3. SPM is a computational depth-reverse process in which original EIs are convertible to ones recorded at the different pickup distances. As shown in Fig. 3, the EIs recorded at the long distance can be converted to ones recorded near lenslet array. This effect can give us the movement of the output plane in CIIR method for 3D objects as shown in Fig. 3. Therefore we can obtain the resolution-enhanced plane image by reducing the interference problem from the magnification process.

To understand the principle of SMP, we consider an integral imaging system as shown in Fig. 4. SPM is a computational pseudoscopic–orthoscopic conversion technique [24]. The depth conversion in SPM involves a two-step recording process. In the first step, the 3D object is recorded as the first EIs. By using the recorded EIs, a 3D image is reconstructed at the distance it was captured. The reconstructed 3D image is then recorded again by a similar pickup system to produce new EIs. Here SPM is implemented using a direct pixel-mapping process by using the first recorded EIs denoted by E. The conversion process is done digitally to produce the second set of EIs. The SPM algorithm for the one-dimensional case is formulated as

$$T_i^j = E_k^l, \tag{4}$$

where

$$l = (V+1) - j,$$
$$k = \begin{cases} i + U/2 - j & \text{if } U \text{ is even} \\ i + (U+1)/2 - j & \text{if } U \text{ is odd} \end{cases}. \tag{5}$$

In Eq. (4), T is the output of E after applying the SPM. The subscripts i and k are corresponding to the EI number, and j and l are the pixel number in the given EI, respectively. The values U and V are the total number of EIs and the total pixels per EI, respectively. We set T_i^j equal to zero if the corresponding $k < 1$ or $k > U$. The effective distance of SPM is given as

$$d = U \times g, \tag{6}$$

where g is the focal length of the lenslet array. In the reconstruction process, we assume the effective distance d of SPM is the longest reconstruction distance for the plane images.

B. Two-Stage Computational Integral Imaging Reconstruction System

For the effective use of the SPM-based CIIR method, we propose a two-stage CIIR method by the combined use of the conventional CIIR and the SPM-based one. The conventional CIIR method is applied over a short distance range, while the SPM-based CIIR is used over a long distance range. The schematic configuration of two-stage CIIR is shown in Fig. 5. Suppose the virtual pinhole array is located at $z = 0$, and the reconstructed images are considered with the effective distance d for SPM. The first CIIR method is identical with the conventional one, as shown in Fig. 5(b). The images are reconstructed plane by plane until the distance $d/2$. On the other hand, the second CIIR using SPM is used when

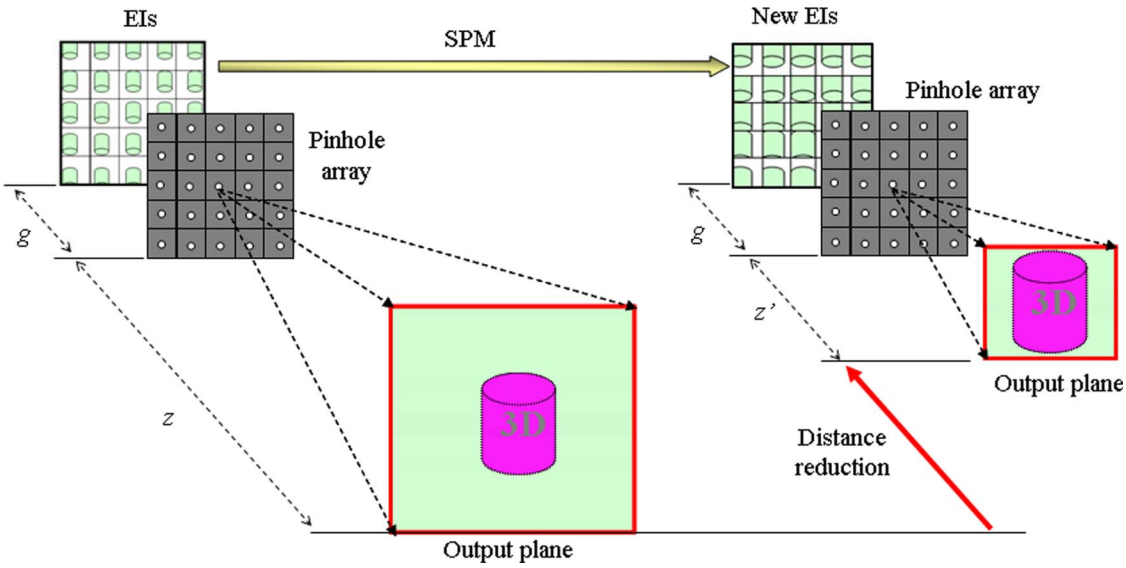

Fig. 3. (Color online) Principle of CIIR by use of SPM.

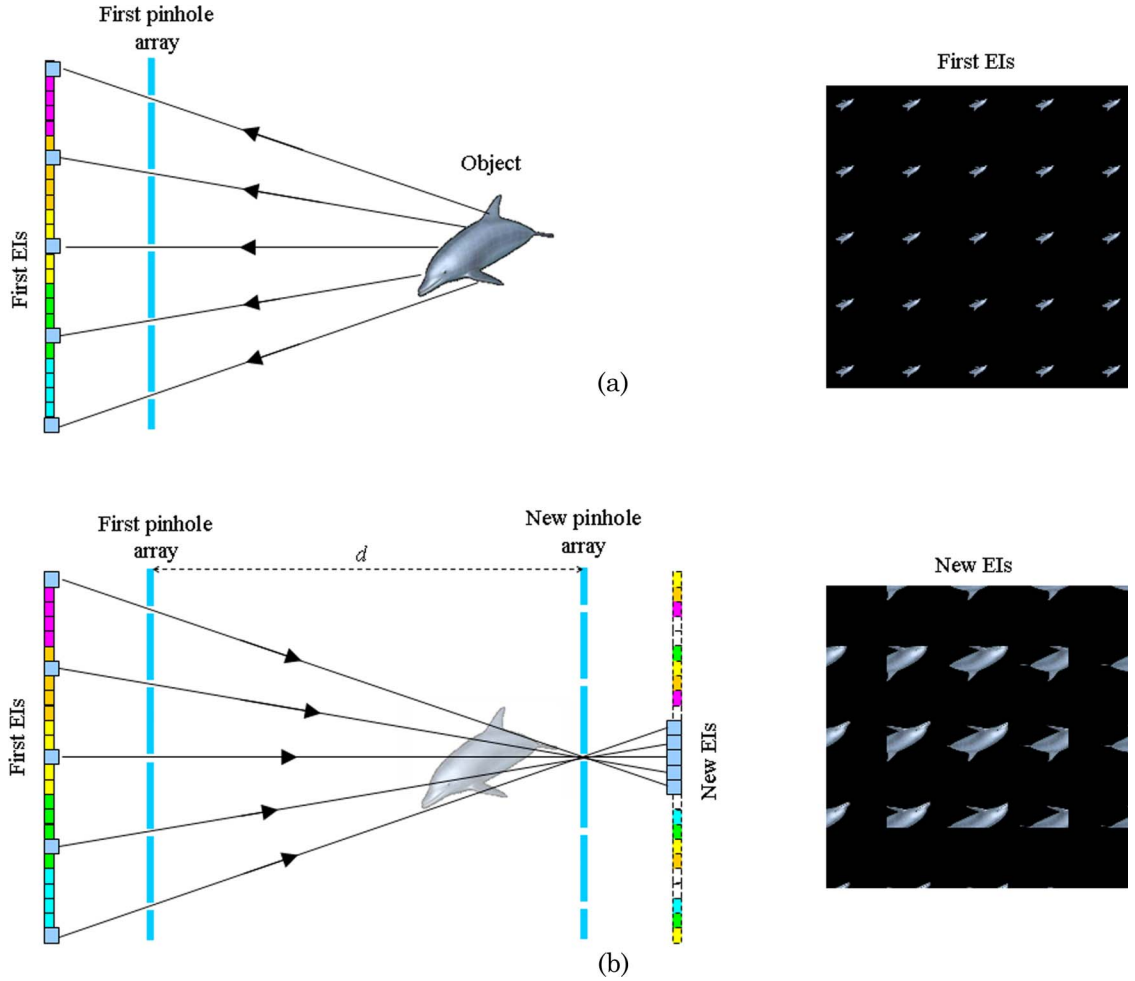

Fig. 4. (Color online) Principle of SMP with two-step recording process: (a) recording of the first EIs and (b) recording of new EIs using SPM.

$z > d/2$. The new EIs are generated by SPM and located at $z = d + g$. The second virtual pinhole array is located at $z = d$. In this case, its plane images are reconstructed in the reverse way. Because of the depth-reverse property of SPM, the reconstruction distance z of a plane image is changed in the second CIIR method. The new distance is given by

$$z' = d - z. \tag{7}$$

The new distance z' allows the plane image to be reconstructed at shorter distance, which reduces resolution degradation of the reconstructed plane image.

4. Experiments and Results

A. Computational Experiments for Image Quality

We carried out computational experiments with a test plane image to objectively evaluate the performance of the proposed two-stage CIIR method. Figure 6 illustrates our experimental setup of computational tests, in which we modeled the symmetric structure between the pickup and the reconstruction process. This is that the clear image of test plane image is reconstructed at the same distance. A virtual pinhole array is composed of 35×35 pinholes, and it is located at $z = 0$ mm. The interval between pinholes is 1.08 mm, and the gap g between the EIs and the pinhole array is 3 mm. The size of test image named "dolphin" is 1050×1050 pixels. After a test image is located at distance z, its EIs are synthesized by the computational pickup based on the simple ray geometric analysis [17]. The number of entire EIs is $U \times U = 35 \times 35$, and each EI has $V \times V = 30 \times 30$ pixels. Then the synthesized EIs are applied to both the conventional CIIR method and the two-stage CIIR method. The plane images reconstructed using the conventional CIIR according to the different distance z are shown in Fig. 7(a). To reconstruct plane images in the two-stage CIIR method, an SPM algorithm was applied to the synthesized EIs. Using Eq. (6), the effective distance was 105 mm. Then the second virtual pinhole array was located at $z = 105$ mm, and the new EIs were obtained at $z = 108$ mm. Both original EIs and newly modified EIs were used in our two-stage CIIR method. The reconstructed images according to the distance are shown in Fig. 7(b).

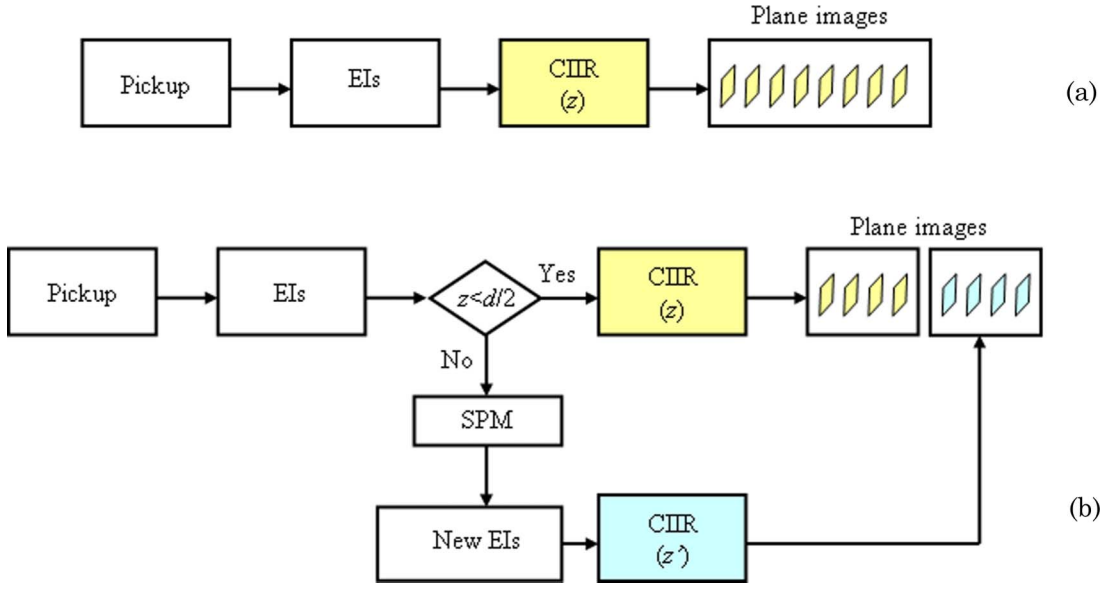

Fig. 5. (Color online) (a) Block diagram of the conventional CIIR system and (b) block diagram of the proposed CIIR system.

To quantitatively evaluate our CIIR method, the peak-to-peak signal-to-noise ratio (PSNR) is employed as an image quality measure. We calculate PSNRs between an original test image $O(x,y)$ and its reconstructed plane image $R^z_{\text{normal}}(x,y)$. The PSNR is defined as

$$\text{PSNR} = 10\log_{10}\frac{255^2}{\text{MSE}}, \tag{8}$$

and MSE is given by

$$\text{MSE} = \frac{1}{PQ}\sum_{x=1}^{P}\sum_{y=1}^{Q}[O(x,y) - R^z_{\text{normal}}(x,y)]^2. \tag{9}$$

The PNSR values calculated for both reconstructed plane images according to the distance are presented in Fig. 8. From the results of Figs. 7 and 8, it is easily seen that the visual quality of the plane images that is reconstructed on a large distance range ($z > 52.5$ mm) by our method outperforms that of the plane image that is reconstructed by the conventional method.

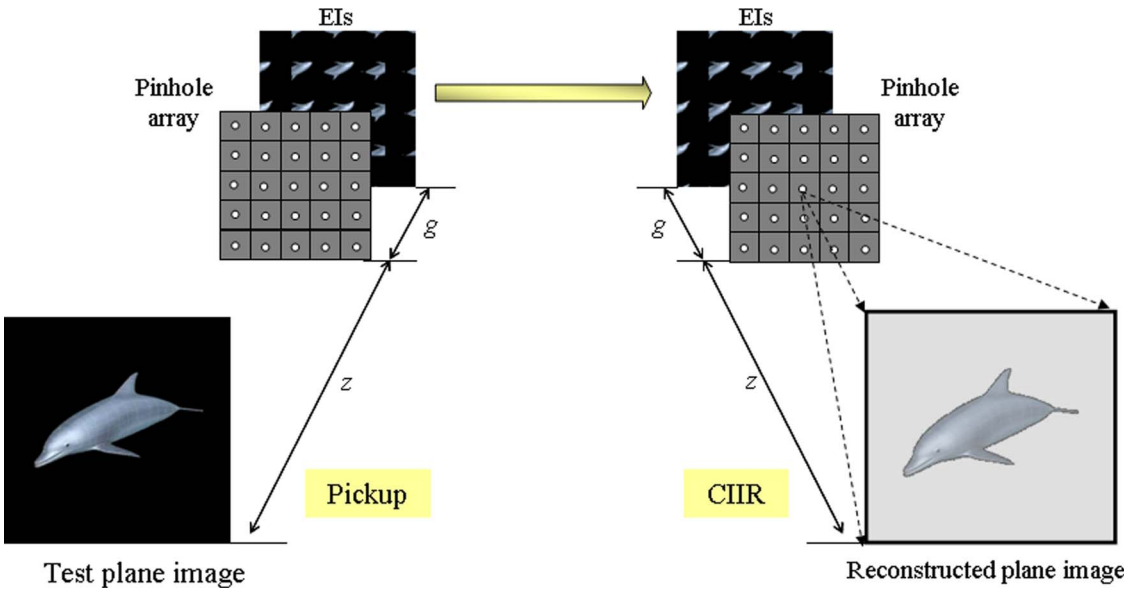

Fig. 6. (Color online) Experimental structure for calculating PSNR.

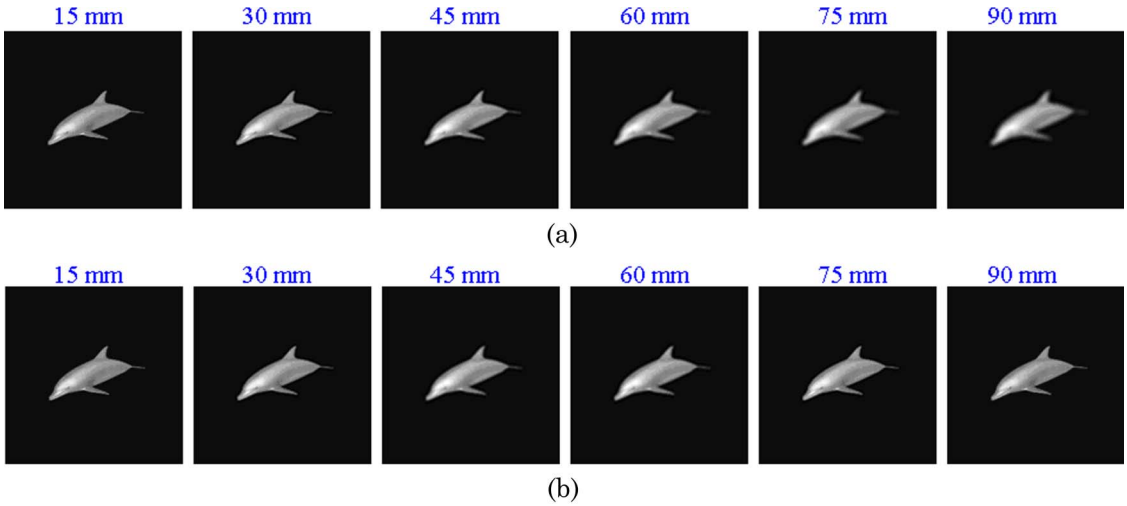

Fig. 7. (Color online) Reconstructed plane images according to distance z: (a) conventional method and (b) proposed method.

B. Experiments for Partially Occluded Three-Dimensional Objects

Next we carried out experiments for partially occluded 3D object reconstruction, which is our good application, because the object to be recognized is always located at a far distance compared to the occlusion, using the proposed two-stage CIIR method. The experimental setup is shown in Fig. 9. We tested four kinds of test image sets as shown in Fig. 10. The test images captured from real objects are shown in Fig. 10(d). In Fig. 9, the original images are used as the template to calculate the PSNR value. The target 3D objects, which are composed of occlusion plane image and object plane image to be recognized, were tested at various distances. In general, objects are behind the occlusion. The pickup in Fig. 9 captures them as the EIs of the target objects, which were captured through a pinhole array by using the computer-generated pickup method. The pinhole array used in these experiments consists of 35 × 35 pinholes, and its pinhole interval is 1.08 mm. The synthesized EIs have 1050 × 1050 pixels, and each EI is composed of 30 × 30 pixels. Examples of the synthesized EIs are shown in Fig. 11(a) when occlusion and object were located at $z = 15$ and 75 mm, respectively. On the other hand, the new EIs after the SPM process are shown in Fig. 11(b). It is seen that the EIs for the 3D objects are much larger than ones of occlusion. This can give us the resolution-enhanced plane images by reducing the interference noise in CIIR

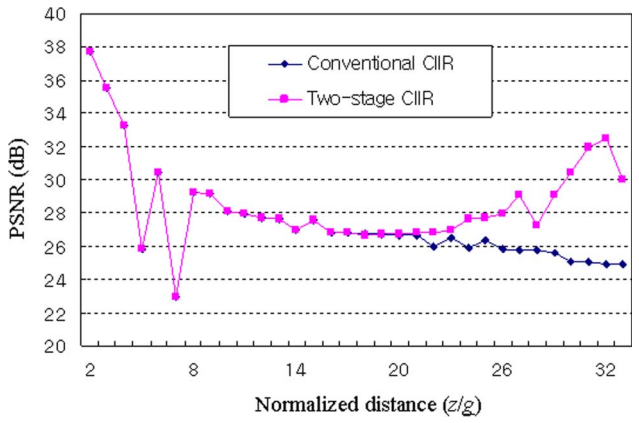

Fig. 8. (Color online) PSNR results for reconstructed plane images.

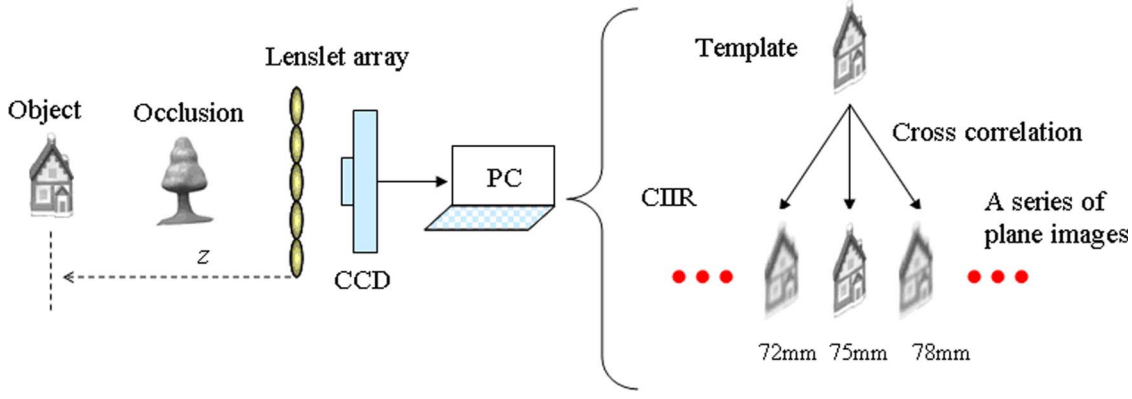

Fig. 9. (Color online) Experimental setup for partially occluded 3D objects.

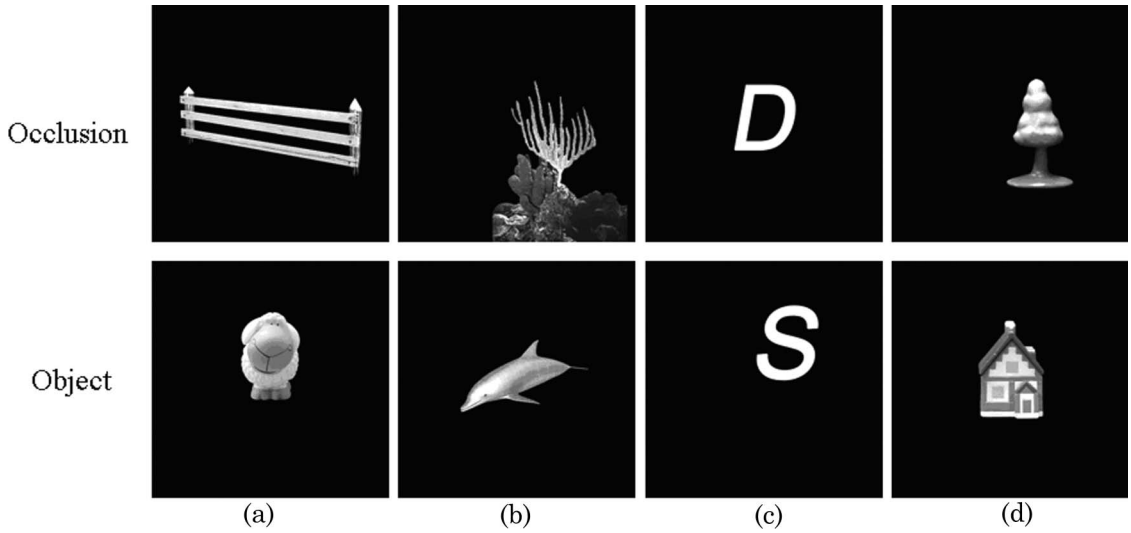

Fig. 10. Four kinds of experimental test images.

process. To obtain plane images of target objects for object correlation, the EIs were applied to both the conventional and our two-stage CIIR method.

To show the characteristics of the proposed method for 3D object recognition, we calculated the PSNR between original object and reconstructed plane

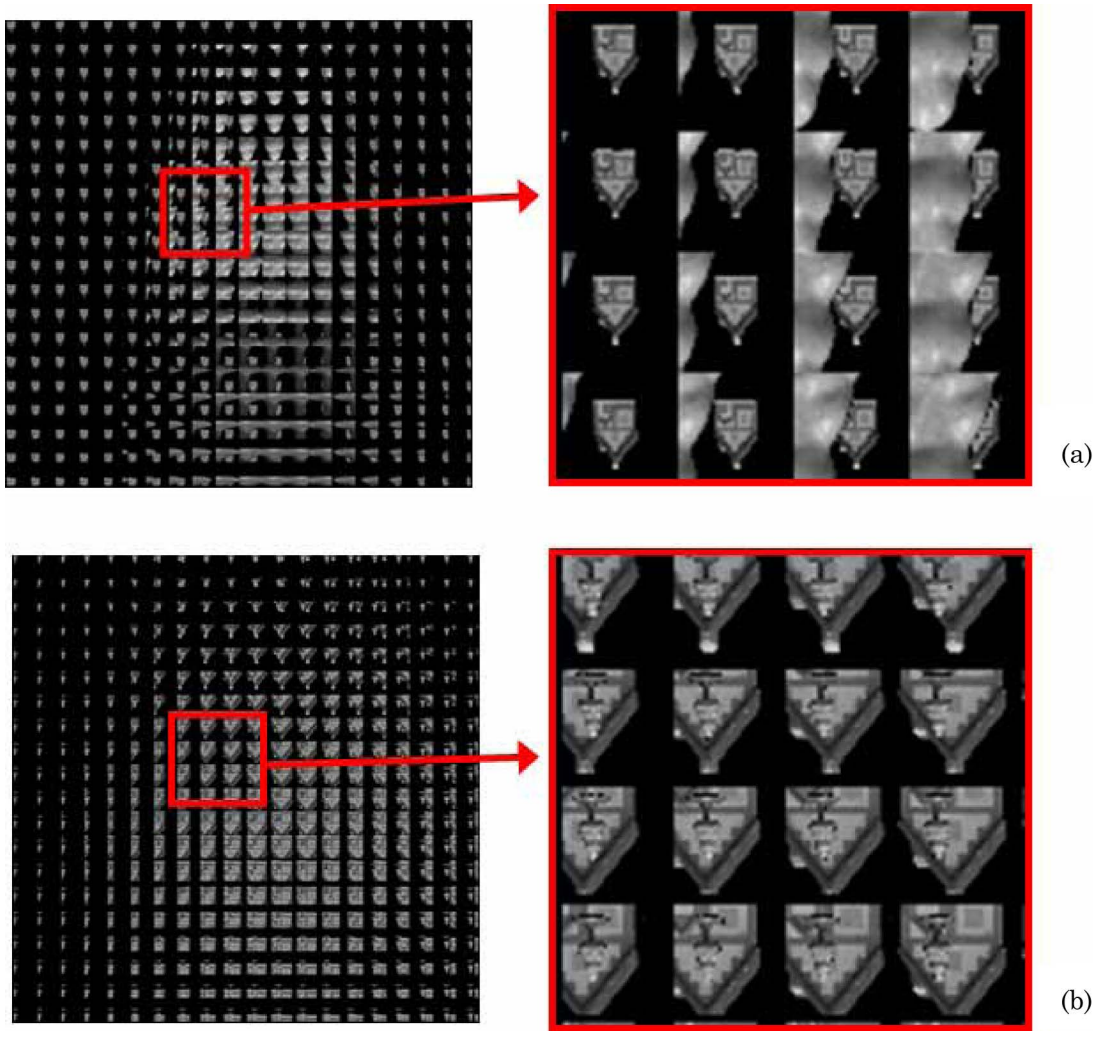

Fig. 11. (Color online) EIs and enlarged images of "tree" and "house" test images: (a) original images and (b) new images after SPM.

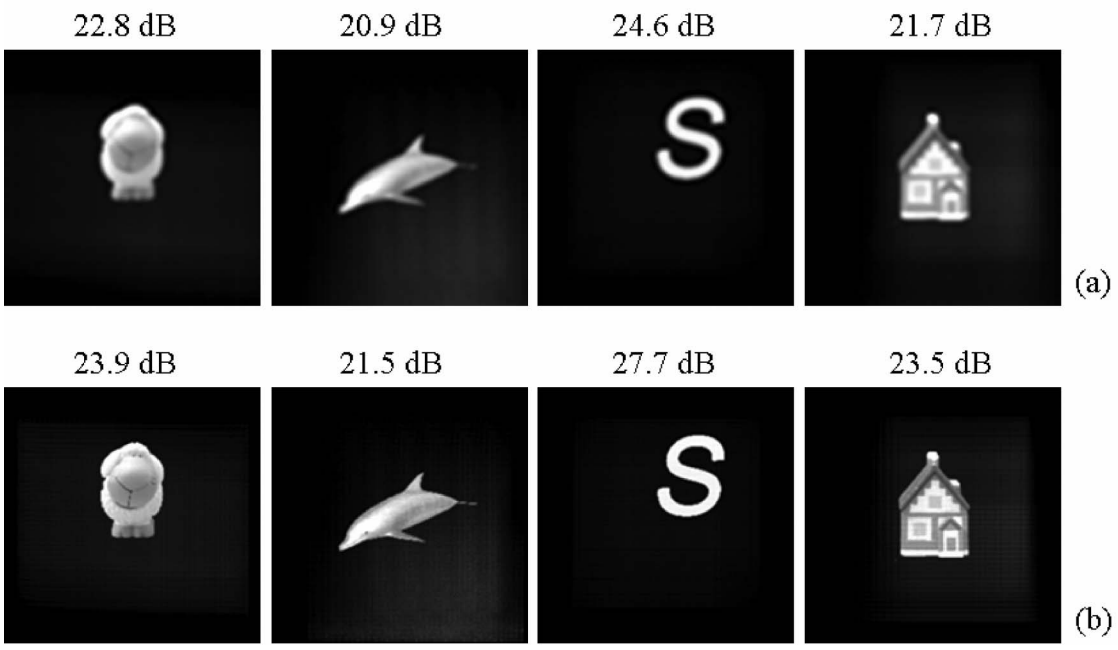

Fig. 12. Reconstructed images and PSNR results: (a) conventional method and (b) proposed two-stage method.

images. The PSNR results are presented in the top of each image as shown in Fig. 12. The results of Fig. 12 indicate that the proposed method can improve the image quality of reconstructed plane images by an average of 1.65 dB. This implies that the proposed method can help us to recognize partially occluded 3D objects.

5. Conclusion

In conclusion, we proposed a two-stage CIIR method to improve the performance of a plane image reconstruction. First we introduced a SPM-based CIIR method, which is a computational process in which EIs recorded at long distance are convertible to ones recorded near the lenslet array. Using this SPM-based CIIR, we designed a two-stage CIIR method. Here the conventional CIIR method was applied over a short distance range, while the proposed CIIR based on SPM was used over a long distance range. In order to verify our proposed method, we carried out some experiments. From the experimental results, we show that the proposed method can provide the improved resolution of the reconstructed plane images. It was also shown that this can be usefully applied to the partially occluded 3D object recognition.

This research was supported by the Ministry of Knowledge Economy (MKE), Korea, under the Information Technology Research Center (ITRC) support program supervised by the Institute of Information Technology Assessment (IITA) (IITA-2008-C1090-0801-0018).

References

1. G. Lippmann, "La photographic intergrale," C. R. Acad. Sci. **146**, 446–451 (1908).
2. A. Stern and B. Javidi, "Three-dimensional image sensing, visualization, and processing using integral imaging," Proc. IEEE **94**, 591–607 (2006).
3. B. Javidi and S.-H. Hong, "Three-dimensional holographic image sensing and integral imaging display," J. Display Technol. **1**, 341–346 (2005).
4. F. Okano, H. Hoshino, J. Arai, and I. Yuyama, "Real-time pick-up method for a three-dimensional image based on integral photography," Appl. Opt. **36**, 1598–1603 (1997).
5. J.-S. Jang and B. Javidi, "Improved viewing resolution of three-dimensional integral imaging by use of nonstationary micro-optics," Opt. Lett. **27**, 324–326 (2002).
6. B. Lee, S. Jung, and J.-H. Park, "Viewing-angle-enhanced integral imaging by lens switching," Opt. Lett. **27**, 818–820 (2002).
7. D.-H. Shin, B. Lee, and E.-S. Kim, "Multidirectional curved integral imaging with large depth by additional use of a large-aperture lens," Appl. Opt. **45**, 7375–7381 (2006).
8. R. Ng, M. Levoy, M. Bredif, G. Duval, M. Horowitz, and P. Hanrahan, "Light field photography with a handheld plenoptic camera," Computer Science Technical Report CSTR 2005-02 (Stanford University, 2005).
9. H. Arimoto and B. Javidi, "Integral three-dimensional imaging with digital reconstruction," Opt. Lett. **26**, 157–159 (2001).
10. Y. Frauel and B. Javidi, "Digital three-dimensional image correlation by use of computer-reconstructed integral imaging," Appl. Opt. **41**, 5488–5496 (2002).
11. Y. Frauel and B. Javidi, "Digital three-dimensional object reconstruction and correlation based on integral imaging," Proc. SPIE **5006**, 83–91 (2003).
12. S. Kishk and B. Javidi, "Improved resolution 3D object sensing and recognition using time multiplexed computational integral imaging," Opt. Express **11**, 3528–3541 (2003).
13. S.-H. Hong, J.-S. Jang, and B. Javidi, "Three-dimensional volumetric object reconstruction using computational integral imaging," Opt. Express **12**, 483–491 (2004).
14. S.-H. Hong and B. Javidi, "Improved resolution 3D object reconstruction using computational integral imaging with time multiplexing," Opt. Express **12**, 4579–4588 (2004).

15. Y.-W. Song, B. Javidi, and F. Jin, "3D object scaling in integral imaging display by varying the spatial ray sampling rate," Opt. Express **13**, 3242–3251 (2005).
16. B. Javidi, R. Ponce-Díaz, and S.-H. Hong, "Three-dimensional recognition of occluded objects by using computational integral imaging," Opt. Lett. **31**, 1106–1108 (2006).
17. S.-H. Hong and B. Javidi, "Distortion-tolerant 3D recognition of occluded objects using computational integral imaging," Opt. Express **14**, 12085–12095 (2006).
18. H. Yoo and D.-H. Shin, "Improved analysis on the signal property of computational integral imaging system," Opt. Express **15**, 14107–14114 (2007).
19. D.-H. Shin and H. Yoo, "Image quality enhancement in 3D computational integral imaging by use of interpolation methods," Opt. Express **15**, 12039–12049 (2007).
20. J.-S. Park, D.-C. Hwang, D.-H. Shin, and E.-S. Kim, "Resolution-enhanced 3D image correlator using computationally reconstructed integral images," Opt. Commun. **276**, 72–79 (2007).
21. S. Yeom, B. Javidi, and E. Watson, "Three-dimensional distortion-tolerant object recognition using photon-counting integral imaging," Opt. Express **15**, 1513–1533 (2007).
22. D.-C. Hwang, K.-J. Lee, S.-C. Kim, and E.-S. Kim, "Extraction of location coordinates of 3-D objects from computationally reconstructed integral images basing on a blur metric," Opt. Express **16**, 3623–3635 (2008).
23. D.-H. Shin and H. Yoo, "Scale-variant magnification for computational integral imaging and its application to 3D object correlator," Opt. Express **16**, 8855–8867 (2008).
24. M. Martinez-Corral, B. Javidi, R. Martínez-Cuenca, and G. Saavedra, "Formation of real, orthoscopic integral images by smart pixel mapping," Opt. Express **13**, 9175–9180 (2005).